BRIEF REPORT

Frameless Robot-Assisted Asleep Centromedian Thalamic Nucleus Deep Brain Stimulation Surgery in Patients with Drug-Resistant Epilepsy: Technical Description and Short-Term Clinical Results

Changquan Wang · Jing Hong · Ziyu Mao · Wenze Chen ·

Bin Chen · Wenzhen Chen · Xiaolai Ye · Chencheng Zhang ·

Yong Lu · Qiangqiang Liu (iD) · Jiwen Xu

ABSTRACT

Introduction: This purpose of this work is to give a detailed description of a surgical technique for frameless robot-assisted asleep deep brain stimulation (DBS) of the centromedian thalamic nucleus (CMT) in drug-resistant epilepsy (DRE).

Methods: Ten consecutively enrolled patients who underwent CMT-DBS were included in the study. The FreeSurfer "Thalamic Kernel

Changquan Wang and Jing Hong contributed equally.

C. Wang · J. Hong · Z. Mao · W. Chen · B. Chen ·
W. Chen · X. Ye · Y. Lu · Q. Liu (✉) · J. Xu (✉)
Clinical Neuroscience Center, Ruijin Hospital
Luwan Branch, Shanghai Jiao Tong University
School of Medicine, 197 RuiJin Er Road, Shanghai
200025, People's Republic of China
e-mail: windsto@163.com

J. Xu
e-mail: xjw88@vip.163.com

J. Hong · W. Chen · X. Ye · Q. Liu · J. Xu
Department of Neurosurgery, Clinical Neuroscience
Center Comprehensive Epilepsy Unit, Ruijin
Hospital, Shanghai Jiao Tong University School of
Medicine, Shanghai, People's Republic of China

C. Zhang
Department of Neurosurgery, Center for Functional
Neurosurgery, Ruijin Hospital, Shanghai Jiao Tong
University School of Medicine, Shanghai, People's
Republic of China

Segmentation" module and experience target coordinates were used for locating the CMT, and quantitative susceptibility mapping (QSM) images were used to check the target. The patient's head was secured with a head clip, and electrode implantation was performed with the assistance of the neurosurgical robot Sinovation®. After opening the dura, the burr hole was continuously flushed with physiological saline to stop air from entering the skull. All procedures were performed under general anesthesia without intraoperative microelectrode recording (MER).

Results: The mean age of the patients at surgery and onset of seizures was 22 years (range 11–41 years) and 11 years (range 1–21 years), respectively. The median duration of seizures before CMT-DBS surgery was 10 years (2–26 years). CMT was successfully segmented, and its position was verified by experience target coordinates and QSM images in all ten patients. The mean surgical time for bilateral CMT-DBS in this cohort was 165 ± 18 min. The mean pneumocephalus volume was 2 cm^3. The median absolute errors in the x-, y-, and z-axes were 0.7 mm, 0.5 mm, and 0.9 mm, respectively. The median Euclidean distance (ED) and radial error (RE) was 1.3 ± 0.5 mm and 1.0 ± 0.3 mm, respectively. No significant difference was found between right- and left-sided electrodes regarding the RE nor the ED. After a mean 12-month follow-up, the average reduction in seizures was 61%, and six patients experienced

a ≥ 50% reduction in seizures, including one patient who had no seizures after the operation. All patients tolerated the anesthesia operation, and no permanent or serious complications were reported.

Conclusions: Frameless robot-assisted asleep surgery is a precise and safe approach for placing CMT electrodes in patients with DRE, shortening the surgery time. The segmentation of the thalamic nuclei enables the precise location of the CMT, and the flow of physiological saline to seal the burr holes is a good way to reduce the influx of air. CMT-DBS is an effective method to reduce seizures.

Keywords: Centromedian thalamic nucleus; Deep brain stimulation; Drug-resistant epilepsy; Robotics; Frameless; Stereotaxic techniques

---

Key Summary Points

This is the first article to present robot surgery technology for centromedian thalamic nucleus deep brain stimulation (CMT-DBS)

Frameless asleep robot-assisted surgery is an accurate and safe approach to CMT-DBS placement, shortening the surgery time

The segmentation of the thalamic nuclei enables the precise location of the CMT

CMT-DBS can effectively reduce seizures, but may not be effective for focal to bilateral tonic–clonic seizures (FBTC)

INTRODUCTION

Epilepsy is a neurological disorder that reduces quality of life, increases costs to society, and increases the risk of dying [1]. The prevalence of epilepsy has been estimated at nearly 1% of the worldwide population [2]. About 36% of patients have uncontrolled seizures, despite optimized antiepileptic drug (AED) treatment, and are consequently diagnosed with drug-resistant epilepsy [3]. Following resective surgery, outcomes at 5 years were available for 61.0% of patients with lesions (for example, mesial temporal sclerosis, focal cortical dysplasia, low-grade developmental and epilepsy-associated brain tumors) [4–6]. Unfortunately, there are still many patients with DRE who are not suitable for resective surgery or have failed epilepsy surgery [6]. For these patients, neurostimulation therapies and a ketogenic diet are alternative options.

Deep brain stimulation (DBS) is an effective and safe neurostimulation therapy for patients with drug-resistant epilepsy (DRE) [7, 8]. In a recent meta-analysis, the mean seizure reduction after stimulation of the anterior thalamic nucleus, centromedian thalamic nucleus (CMT), and hippocampus was 60.8%, 73.4%, and 67.8%, respectively [9]. Especially for patients with generalized seizures and Lennox–Gastaut syndrome, many studies suggest that CMT-DBS has a favorable effect [7, 10, 11].

Effective stimulation depends on the accurate implantation of deep electrodes with the assistance of a stereotactic system. However, the clinical outcome is related to the precision and accuracy of electrode implantation and varies among studies [12–14]. Accurate target location and precise electrode implantation are the most important factors in achieving a satisfactory curative effect. The CMT is not directly visible using structural neuroimaging, so prior studies have targeted CMT using the Schaltenbrand atlas or empirical coordinates [15–17]. These approaches could lead to gross misplacement of electrodes outside the CMT in some cases [10, 12].

Many techniques have been used to improve the accuracy of electrode implantation. Frame-based stereotaxic surgery has been widely practiced around the world for more than 30 years [18]. However, in the last decade, the popularity and number of robot-assisted DBS surgeries performed have progressively increased. Despite many objections, some studies have shown that robot-assisted surgery is as accurate as or even better than conventional frame-based stereotactic surgery [19, 20]. Those experiments used the subthalamic nucleus and internal globus

pallidus as targets for Parkinson's disease and essential tremor. Currently, there are fewer reports on robot-assisted surgery for CMT-DBS [21]. The purpose of the present study is to provide a detailed description of the frameless robot-assisted asleep CMT-DBS procedure and short-term clinical results for DRE.

METHODS

Study Participants

Our study included enrolled patients who underwent CMT-DBS at the epilepsy centers of the Ruijin Hospital in China between September 2021 and May 2022. All cases were discussed at a multi-disciplinary conference on epilepsy, and all patients were diagnosed with DRE with Lennox–Gastaut syndrome (LGS), generalized-onset seizures (include atypical absences, atonic seizures, bilateral tonic–clonic seizures, myoclonic seizures, tonic seizures), focal to bilateral tonic–clonic seizures (FBTC), and focal-onset motor seizures. This study was approved by the Ruijin Hospital Luwan Branch Ethics Committee, Shanghai JiaoTong University School of Medicine, and was completed in accordance with the Helsinki Declaration. All patients gave their written informed consent prior to surgery. Consent was also recieved from the patients for the publication of any identifiable infomation, including patient photographs.

Neuroimaging Acquisition

Preoperative magnetic resonance (MR) scanning to localize the CMT was performed in all patients several days before surgery. The MR study included T1 magnetization-prepared rapid acquisition gradient echo (MPRAGE) (voxel size $0.5 \times 0.5 \times 0.5$ mm), T2 sequences (voxel size $0.3 \times 0.5 \times 0.3$ mm), quantitative susceptibility mapping (QSM) (voxel size $1 \times 1 \times 2$ mm), and phase contrast magnetic resonance angiography (PCA) (voxel size $0.37 \times 0.37 \times 0.37$ mm) using a 3.0-T scanner (uMR 890, United Imaging Healthcare, Shanghai, China) with a dedicated 64-channel head coil.

Surgical Plan

Iglesias et al. [22] present a probabilistic atlas of the thalamic nuclei built using ex vivo brain MRI scans and histological data, as well as the application of the atlas to individualized MRI segmentation. The target location for each electrode was determined using the module "Segmentation of thalamic nuclei" in FreeSurfer (version 7.1) [22]. This procedure took more than 10 min after the T1 MPRAGE images had been analyzed with the main FreeSurfer stream (the code "recon-all") [23]. Then we obtained the probability map files of the thalamic nucleus (ThalamicNuclei.v12.T1.FSvoxelSpace.mgz), which contain 25 different thalamic nuclei. This method has been proven to be an effective method of thalamic segmentation [24]. It should be noted that if the "recon-all" process fails due to brain abnormalities, the "Segmentation of thalamic nuclei" process cannot be performed. The map files stored the discrete segmentation volume in the FreeSurfer voxel space, just as for the T1 MPRAGE images. 3D slicer (version 4.10.2) was used to convert the map file and pial surfaces to nifti format files [25].

The Sinovation® surgical planning system (version 2.0.1.2; a portable computer; Sinovation, Beijing, China) was utilized to create the surgical plan. The map files and pial surfaces can be reconstructed for three-dimensional (3D) models in the planning system, which is convenient for target and trajectory planning. T1 MPRAGE images, PCA images, and converted files were imported into the surgical planning system. The target points were located according to the position of the CMT in the segmentation nucleus. Experience target coordinates based on the anterior commissure–posterior commissure (AC–PC) coordinates and QSM were also used to check the targets. The experience coordinates for CMT were located 10 mm lateral to the midline, 1 mm anterior to the PC, and in the AC–PC plane [10, 21, 26]. The entry points were planned so as to avoid sulci, ventricles, vascular structures, as well as the segmented thalamic nuclei in structural images and three-dimensional models to ensure that more electrode contacts passed through the

CMT. Image processing procedures and results are shown in Figs. 1 and 2. Image verification of the segmented thalamic nucleus is shown in Fig. 3.

Surgical Procedure

After trajectory planning, leads were implanted using the Sinovation® neurosurgical robot system (Sinovation, Beijing, China). On the day of surgery, five bone fiducial markers were inserted into the skull under local anesthesia and to allow frameless registration. Then, the patients underwent a head computed tomography (CT) scan (voxel size 0.43 × 0.43 × 1.0 mm). The CT images were imported into the surgical planning system and fused to the T1 MPRAGE images.

All procedures were performed under general anesthesia without intraoperative microelectrode recording (MER). The patient was placed in the supine position and the head was rigidly fixed by a DORO QR3 skull clamp with three head fixation points. After the connecting rod of the robot was connected and fixed with the skull clamp, registration was started. The four bone fiducial markers were used for registration and the fifth bone fiducial marker was used for verification. In our procedure, registration accuracy was considered acceptable when it was below 0.30 mm. If values exceeded 0.30 mm during registration, the registration was repeated (Fig. 4).

Under the guidance of the pointer, the scalp was opened and a frontal burr hole was drilled by an electric drill co-axial to the trajectory. Intraoperative verification was performed again after the skin incision and skull hole drilling. If the verification error had increased, intraoperative registration was repeated.
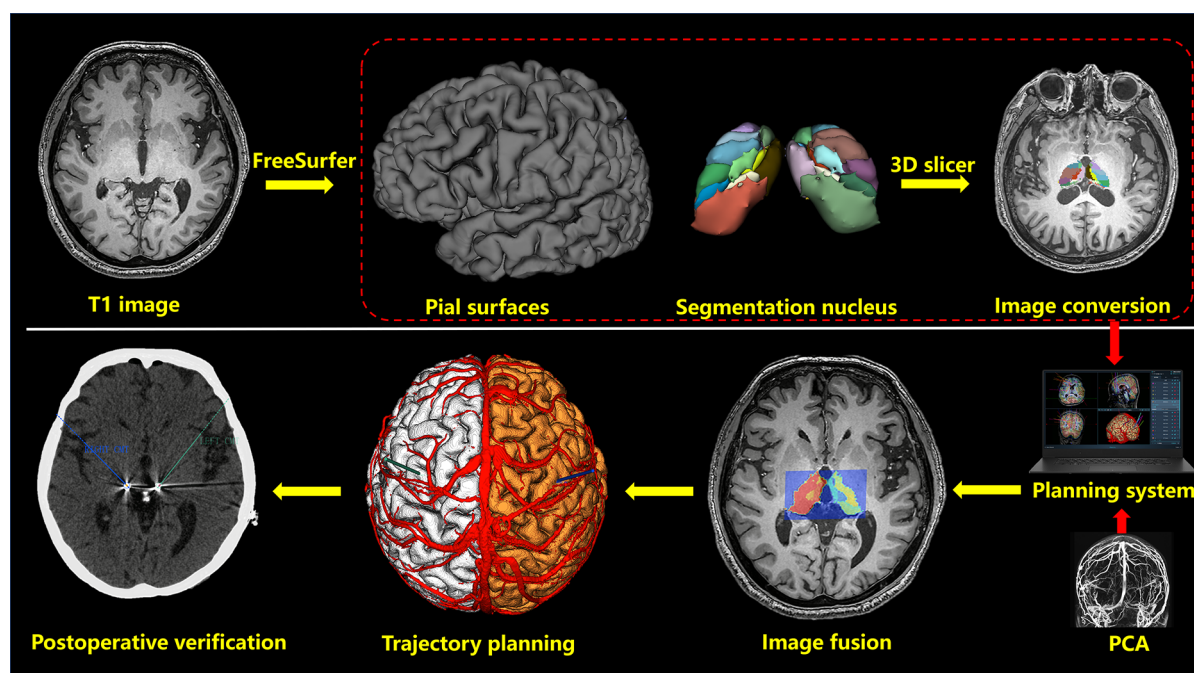

Fig. 1 Image processing procedures. The T1 image is processed with FreeSurfer to obtain pial surfaces and segmentation thalamic nuclei. Then, these data are imported into 3D Slicer for format conversion. The results (in the *dotted red box*) are imported into the Sinovation® surgical planning system together with the phase contrast magnetic resonance angiography (PCA) image. After image fusion and 3D model reconstruction, surgical planning and then postoperative electrode verification are carried out in the Sinovation® surgical planning system
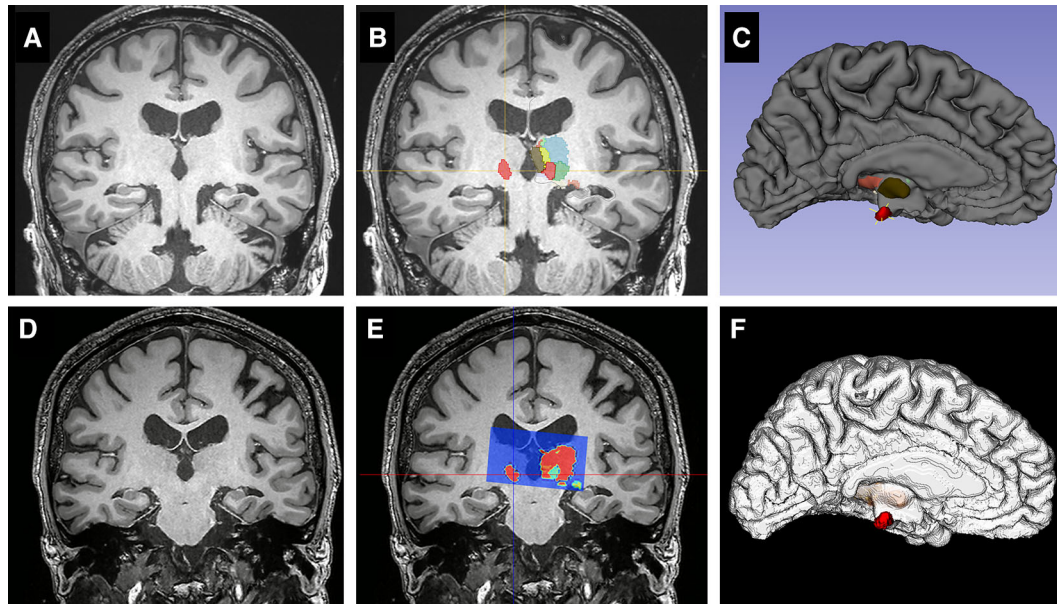
Fig. 2 The image and models of thalamic nuclei and the pial surface. **A–C** Screenshots from 3D Slicer. **D–F** Screenshots from the Sinovation® surgical planning system. **A** Coronal view in T1 MPRAGE images and **D** coronal view in T1 MPRAGE in the AC-PC plane; the CMT is not visible in the T1 image. **B**, **E** Segmented thalamic nuclei are shown in a pseudo-color image and in a fusion image combining the pseudo-color image with a T1 image. The *crosses* reference the right CMT and the complete segmented nuclei are covered on the left thalamus. **C**, **F** Left hemispheric model of the pial surface and the 3D model of the right CMT (*red*)

In order to avoid cerebrospinal fluid (CSF) leakage during the surgery, a small incision in the dura and leptomeninx was made by electrotome. After opening the dura, the burr hole was continuously flushed with physiological saline to stop air from entering the skull. The robotic arm was then deployed and a microdriver (microTargeting™ Platform, FHC, Inc.) for lead implantation was attached to it. A blunt stylet was introduced into the guide tube and gently lowered down to 10 mm above the target. Then, a quadripolar non-directional DBS lead (3389, Medtronic, Inc.) was inserted into the target by microdriver under the guidance of a blunt stylet and secured on the skull surface by a StimLock burr hole cover.

After the two electrodes were implanted, the robot was removed and the skull clamp with the head was rotated about 45° to the right to facilitate the subsequent procedures. The neurostimulator (ACTIVA™ RC, Medtronic, Inc.) was implanted in the left chest and connected to the electrodes by extension wires. The duration of surgery was calculated from when general anesthesia was induced to when the incision was closed, and included registration, sterilization, and lead and neurostimulator implantation surgery.

Accuracy Measurements

All patients underwent postoperative CT scanning the day after surgery to verify the positions of the DBS electrodes and to identify any signs of intracranial hemorrhage immediately after implantation. The accuracy of each electrode was confirmed by fusing preoperative MR and postoperative CT images in the Sinovation® surgical planning system (Fig. 5). The coordinates of the initially planned target and the actual position of the tip of the lowest DBS contact were obtained and compared, looking at the radial error (RE) and the absolute and directional errors in the *x*-, *y*-, and *z*-axes as well as the Euclidean distance (ED), as described in previous studies [19]. Pneumocephalus may
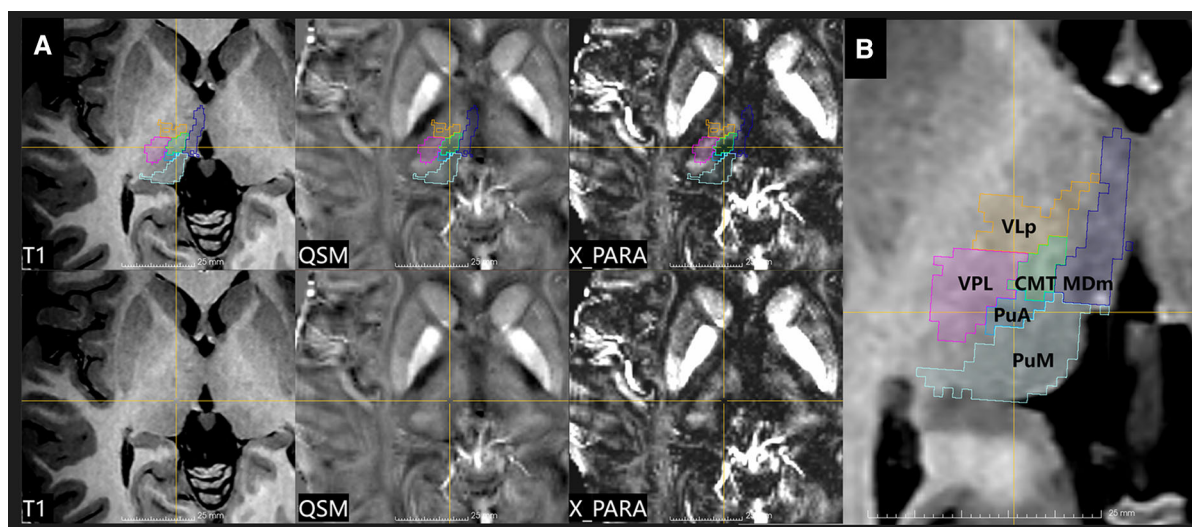
Fig. 3 Image verification of the segmented thalamic nucleus. **A** T1 image (*left*), quantitative susceptibility map (QSM, *middle*), and paramagnetic susceptibility map (X_para, *right*) from patient 8. The *upper image* combines part of the segmented thalamic nucleus, and the *lower image* is the original image. The edge details for the thalamus are more visible in the X_para image compared with other images, especially in CMT (pointed out by the cross). **B** An enlarged view of the thalamic nucleus fused with the T1 image. The boundary of the segmented CMT is close to the result from the QSM. These images are from screenshots from 3D Slicer. *CMT* centromedian thalamic nucleus, *MDm* mediodorsal medial magnocellular, *PuA* pulvinar anterior, *PuM* pulvinar medial, *VLp* ventral lateral posterior, *VPL* ventral posterolateral

lead to a brain shift, thus affecting the accuracy of electrode implantation. Therefore, we counted the pneumocephalus volume in the postoperative CT.

Collected Data and Statistical Analysis

Demographics, medical history, and preoperative and postoperative imaging were collected for all patients. A daily diary of seizures was completed by the patient or caregiver during the 3 months preceding DBS and continuously after the start of stimulation. The coordinates of the planned target and actual positions and the values of RE, ED, depth error, pneumocephalus volume, and duration of surgery were collected. Results were expressed as mean ± standard deviation of the mean. The two-sample t-test was used for comparing categorical variables. p values < 0.05 were considered significant. Correlations were tested using the Pearson correlation coefficient. The data were entered into a Microsoft Excel worksheet and statistically analyzed using Stata 11 (StataCorp, College Station, TX, USA).

RESULTS

Population Data

A total of ten consecutive patients (eight males and two females) with drug-resistant epilepsy underwent frameless robot-assisted CMT-DBS. Surgeries took place in a single center and were performed by a single surgeon (Q.Q. Liu). The average age of the patients at surgery was 21.5 ± 9.5 years (mean ± standard deviation; range 11–41 years). The mean age at seizure onset was 10.3 ± 8.4 years (range 1–21 years), and the average duration of seizures prior to CMT-DBS surgery was 11.2 ± 5.5 years (range 2–26 years). Before the operation, 3.3 (range 2–6) AEDs were taken on average. Table 1 presents the demographics and clinical features.
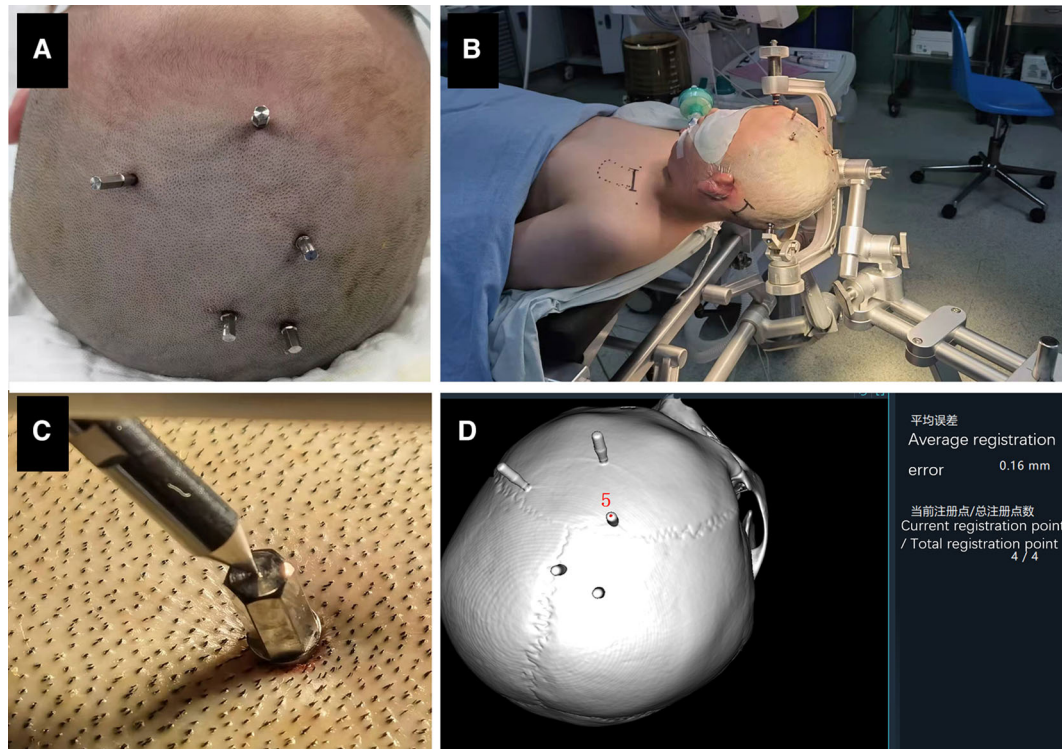
Fig. 4 Patient's position and registration during operation. **A** Photograph after the installation of five bone fiducial markers. **B** The patient is shown placed in a supine position after general anesthesia, with the head fixed using a DORO head frame. After the electrodes have been implanted, the robot is removed, and the patient's head with head frame is rotated about 45° to the right to facilitate the postauricular incision. **C** The registration step. **D** The average registration error was 0.16 mm in this patient. The marker '5' refers to the verification marker

Robot-Assisted DBS Surgery

Thalamic nuclei were successfully segmented and the CMT was finely targeted in all ten patients. The location of the CMT was verified using experience target coordinates and QSM images. CMT-DBS was performed successfully. All patients tolerated the anesthesia operation, and 20 electrodes were implanted. The mean surgical time for bilateral CMT-DBS in this cohort was 165 ± 18 min (range 147–197 min). The pneumocephalus volume in postoperative CT was less than 1 cm^3 (recorded as 1 cm^3) in six patients, and the mean volume for all patients was 2 cm^3 (range 1–7 cm^3). None of the patients presented with intracranial hemorrhage or infection, and no other serious complications were observed.

Accuracy Measurements

The median absolute errors in the x-, y-, and z-axes were 0.7 mm (range 0.1–1.5 mm), 0.5 mm (range 0.0–1.2 mm), and 0.9 mm (range 0.3–1.5 mm), respectively. The median ED was 1.3 ± 0.5 mm (range 0.8–1.9 mm), and the median RE was 1.0 ± 0.3 mm (range 0.2–1.7 mm). There was no significant difference between right- and left-sided electrodes regarding the RE ($p = 0.43$, two-sample t-test), nor the ED ($p = 0.54$). No electrode was readjusted following the postoperative CT scan due to an ED of greater than 2 mm. The accuracy of the electrodes and the surgical times are provided in Table 2. There was no obvious correlation between pneumocephalus volume and implantation accuracy (Fig. 6).
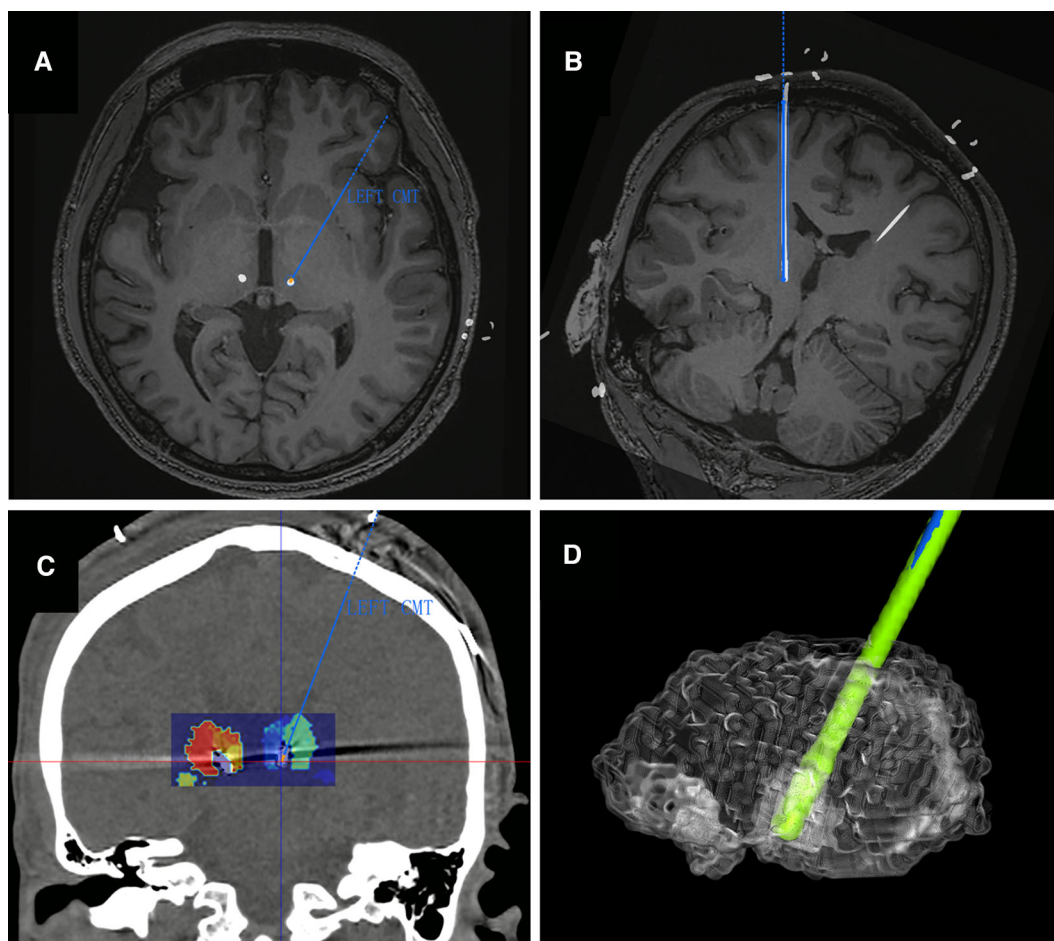
Fig. 5 Postoperative verification. **A**, **B** The fusion image of T1 and postoperative CT in axial and trajectory views. **C** The fusion image of the segmentation of the bilateral thalamus nuclei and postoperative CT in a coronal view. The electrodes pass through the CMT. The *cross* indicates the target of the plan. **D** The 3D model of the thalamic nuclei (*white*) and electrodes (*green*). The *blue line* indicates the trajectory of the left CMT. The fusion step was completed in the Sinovation® surgical planning system

Clinical Results

The DBS system parameters were as follows: bipolar stimulation, current 2–4 V, pulse width 160 μs, frequency 130 Hz. The stimulation was started 1 week after the DBS electrodes were implanted, and seizure reductions occurred in all patients. Six (60%) patients in our group had a ≥ 50% reduction in diary-recorded seizures, including one patient who became seizure free, and the mean seizure reduction was 61% at the last follow-up (mean 12 months, range 6–17 months). At the last follow-up, no changes were made in AEDs for any patient, and all patients received high-frequency stimulation (130 Hz). All patients tolerated the stimulation well, and there was no case in whom stimulation was stopped due to stimulation complications. It was found that a high voltage (more than 5 V) could cause numbness and pain in the contralateral body in all patients. No other serious complications were observed. The seizure type and absolute numbers of seizures per month for all patients are presented in Table 3.

Table 1 Summary of the patients' characteristics

No.	Gender	Age at surgery (years)	Duration of seizures (years)	Age at seizure onset (years)	Antiepileptic drugs
1	Male	41	26	15	CBZ, LCM, LTG, PB, PHT, VPA
2	Male	11	4	7	CBZ, LEV, LCM, OXC
3	Male	17	8	9	LEV, LTG, VPA
4	Male	31	10	21	CBZ, VPA
5	Male	30	22	8	OXC, TPM
6	Male	12	2	10	CBZ, LEV, OXC, PER
7	Male	18	2	16	LEV, LCM, OXC
8	Female	16	15	1	CZP, PER, TPM, VPA
9	Male	17	4	13	PB, PHT, VPA
10	Female	22	10	12	CZP, VPA, ZNS
Mean ± SD		21.5 ± 9.5	10.3 ± 8.4	11.2 ± 5.5	

CBZ carbamazepine, *CZP* clonazepam, *LCM* lacosamide, *LEV* levetiracetam, *LTG* lamotrigine, *LVT* levetiracetam, *OXC* oxcarbazepine, *PER* perampanel, *PB* phenobarbital, *PHT* phenytoin, *SD* standard deviation, *TPM* topiramate, *VPA* valproate, *ZNS* zonisamide

Table 2 Accuracy of electrodes and surgical times

| No.	Surgical time (min)	Pneumocephalus volume (cm³)	Euclidean distance (mm)	Radial error (mm)	Absolute errors (mm)		
					x-axis	*y*-axis	*z*-axis
1	197	7	1.5	1.1	0.45	0.45	1.3
2	176	1	1.25	1	0.6	0.25	1.05
3	186	1	1.7	1.6	0.95	0.9	0.85
4	173	1	1.2	1	0.9	0.25	0.75
5	151	2	1.5	1	1.05	0.8	0.65
6	159	1	1.85	1.5	1.15	0.8	1.15
7	165	1	1.6	1.1	0.7	0.8	1.2
8	139	2	0.9	0.5	0.25	0.1	0.8
9	155	2	0.1	0.7	0.45	0.2	0.8
10	147	1	0.9	0.8	0.4	0.3	0.65
Mean ± SD	164.8 ± 18.2	1.9 ± 1.9	1.3 ± 0.5	1.0 ± 0.3	0.7 ± 0.3	0.5 ± 0.2	0.9 ± 0.2

SD standard deviation
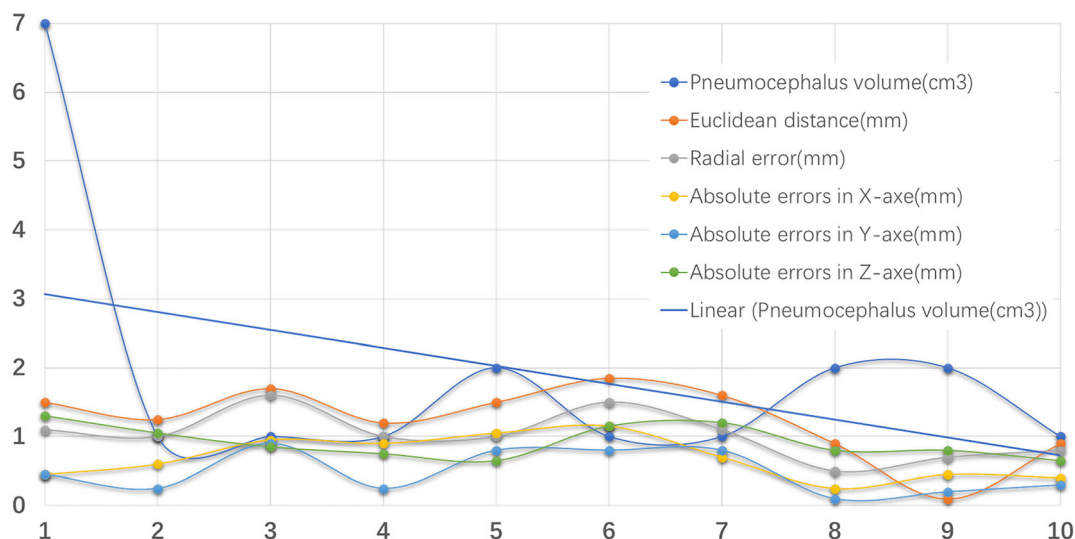
Fig. 6 Connection between pneumocephalic volume and accuracy of electrodes. The *horizontal axis* depicts patients 1 through 10. The correlation coefficients of pneumocephalic volume with Euclidean distance, radial error, and the absolute errors in the *x*-axis, *y*-axis, and *z*-axis were 0.03, − 0.08, − 0.34, − 0.11, and 0.45, respectively. There was no obvious correlation

DISCUSSION

Following the first reports from a Mexican group on the successful management of patients with DRE by bilateral stimulation of the CMT [27, 28], growing evidence during the last 30 years has supported and expanded the application of DBS in DRE [7, 10, 11]. At present, there are few introductions describing how to perform CMT-DBS. This clinical study aimed to evaluate the feasibility of frameless robot-assisted CMT-DBS in a cohort of patients with DRE.

Asleep Surgery

DBS for movement disorders has traditionally relied on awake surgery to facilitate intraoperative monitoring via MER and test stimulation. Although there are still disputes, due to recent advancements in stereotactic techniques, pre- or intraoperative imaging, and incurred cost and risk issues, some operation centers are performing DBS under general anesthesia, and MER may not be a required procedure [19, 21, 29, 30]. Besides, CMT-DBS is a chronic stimulation which cannot produce an immediate effect during intraoperative stimulation. Especially for patients who are very young or have mental retardation, it may be difficult to perform awake surgery. Therefore, epileptic DBS can be operated under anesthesia. Compared with the awake surgery, the asleep surgery exhibited a shorter procedure duration but a similar electrode implantation accuracy and effect on movement disorders [31, 32]. The key aspect of asleep surgery is the use of intraoperative imaging to verify the electrode placement locations without MER or test stimulation [33]. In our study, DBS for epilepsies was performed under general anesthesia without MER and all patients tolerated the operation.

Operation Time

The operation time between when general anesthesia was induced and final closure in our study (165 ± 18 min) is on the lower side of the range reported in previous studies [19, 33, 34]. This may be related to the following factors. First, different studies use different time calculation methods. Some studies calculated the time between patient entry into the operation room and final closure (mean

Table 3 Clinical results after CMT-DBS

No.	Epilepsy syndrome	Seizure type	Seizures before operation (frequency/month)	Seizures after operation (frequency/month)	Follow-up (months)	Stimulation parameters (configuration, voltage, pulse width, frequency, cycling)	Reduction in seizures (%)
1	LGS	AA, AT, T	420	5	17	Bipolar, 2.5 V, 90 μs, 130 Hz, continuous	99
2	LGS-like	AA, T	49	45	17	Bipolar, 3 V, 100 μs, 130 Hz, continuous	8
3	Idiopathic epilepsy	AA, MYO	32	15	15	Bipolar, 2.5 V, 90 μs, 130 Hz, continuous	53
4	Focal epilepsy	FIA, FBTC	5	4	14	Bipolar, 3 V, 90 μs, 130 Hz, continuous	20
5	Focal epilepsy	FIA, FBTC	7	3	14	Bipolar, 3.5 V, 90 μs, 130 Hz, continuous	40
6	Focal epilepsy	FC, FBTC	172	36	12	Bipolar, 3 V, 90 μs, 130 Hz, continuous	79
7	Focal epilepsy	FC, FBTC	561	97	12	Bipolar, 3 V, 90 μs, 130 Hz, continuous	83
8	LGS	AA, T, epileptic spasm	11	6	7	Bipolar, 4 V, 90 μs ,130 Hz, continuous	45
9	Idiopathic epilepsy	AA, GBTCS	5	0	6	Bipolar, 3.5 V, 90 μs, 130 Hz, continuous	100
10	Idiopathic epilepsy	GBTCS	15	2	6	Bipolar, 3.3 V,90 μs, 130 Hz, continuous	87
Mean			128	21	12		61

AA atypical absences, *AT* generalized-onset atonic seizures, *FBTC* focal to bilateral tonic–clonic seizure, *FC* focal-onset clonic seizure, *FIA* focal impaired awareness seizure, *GBTCS* generalized-onset bilateral tonic–clonic seizures, *LGS* Lennox–Gastaut syndrome, *MYO* myoclonic seizures, *T* generalized-onset tonic seizures

280.5 ± 59.2 min, robot-based surgery) [34] or the time between anesthesia induction and the end of anesthesia (mean 447.9 ± 48.4 min, frame-based surgery) [19]. Second, different headsets were used (frameless or frame-based). We used a three-pin skull clamp to fix the patient's head (frameless). The pins were away from the surgical area, and we could finish all the operations at once without removing the skull clamp. Previous studies used a stereotactic frame to fix the patient's head (frame-based).

We should remove the frame after electrode implantation and disinfect again before subsequent stimulator implantation. Third, there is a learning curve when using robots [33, 35, 36]. The registration process and the operation of the software and equipment affect the operation time [19]. We have carried out many DBS and stereotactic electrode implantation operations with robots, so we have passed this learning stage.
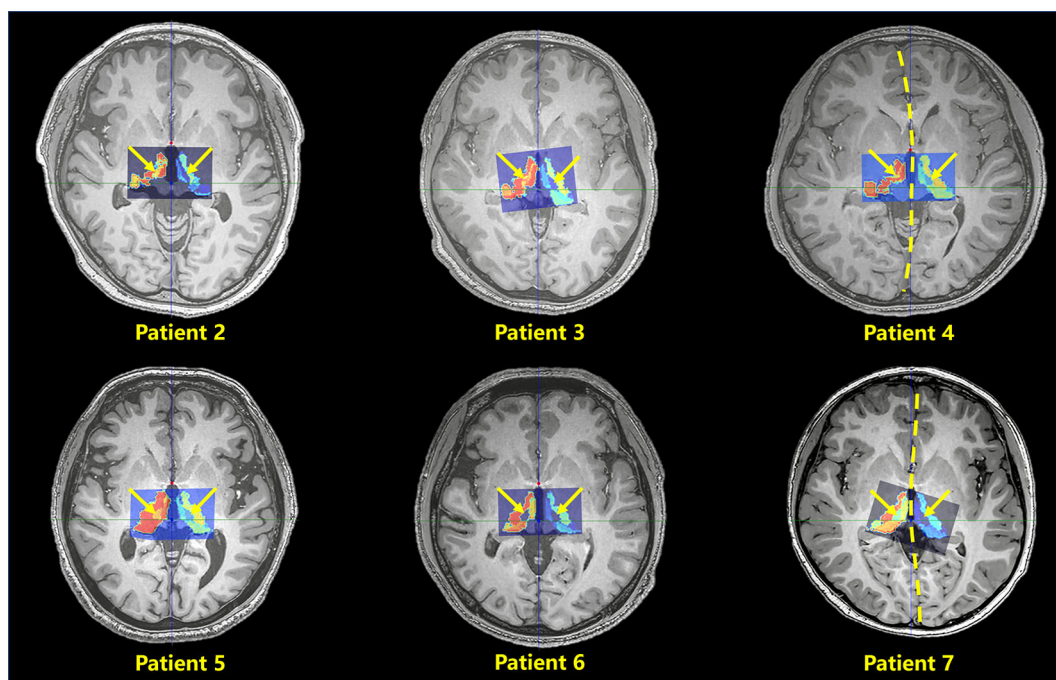
Fig. 7 T1 image fusion with the thalamic nuclei from patients 2 to 7. The bilateral thalamic nuclei are displayed in pseudo-color and merged with the T1 image. The segmented result contains 25 different thalamic nuclei. The *yellow arrow* indicates the position of the CMT. The *dotted yellow lines* indicate bilateral cerebral hemisphere asymmetry in patients 4 and 7. The width of the third ventricle varies greatly among the patients. Iglesias's method successfully locates the CMT and other nuclei in patients with mild bilateral brain asymmetry. All images have been adjusted to the anterior commissure–posterior commissure (AC–PC) plane, and the image center crosshair is located at the PC point

Target Location

Presently it is not possible to locate the CMT using the imaging landmarks provided by CT or MRI [15]. At present, many operations rely on atlas or empirical coordinates (posterior commissure and the plane level, $\sim 10\,mm$ away from the midline). Individual anatomical variation due to a congenital anomaly will lead to electrode misplacement. Unfortunately for patients with an anatomical variation, electrode displacement occurs [37]. Recently, some research has indicated that QSM and magnetization-prepared 2 rapid acquisition gradient echoes (MP2RAGE) are promising methods for improving the visualization of the CMT [12, 38]. These scanning and processing methods are complex and need further verification. Especially in QSM images, although the CMT is visible, it is difficult to distinguish the boundary, as it yields a low signal (Fig. 3).

Thalamus segmentation is another effective way to locate the nuclei [39, 40]. However, these segmentation processes are carried out in the standard space. The results need to be transformed into the individualized space to locate the nuclei. In our study, the position of the segmented CMT in all patients was consistent with the empirical coordinates. Including two patients with anatomical variation, Iglesias's method successfully located the CMT (Fig. 7).

DBS operation requires more electrode contacts to pass through the target. However, CMT experience coordination provides just one point, and we cannot get another point to optimize the electrode trajectory. In the 3D model of CMT and its boundary fused onto structural images, we can directly see the

relationship between the trajectory and the CMT to ensure the operation's success.

Accuracy of the Electrodes

Cerebrospinal fluid leakage and air inflow lead to a nonlinear deformation of the brain (supine position) [41], and the bone drilling may lead to a skull shift [42]. These factors will influence the precise placement of electrodes. The median ED in our study was 1.5 ± 0.3 mm; this value is quite close to those in previous studies [20, 34, 35]. To minimize these errors, the following improvements have been made. First, an excessive dural incision causes excessive cerebrospinal fluid loss, so we use an electrotome to burn a small incision in the dura, sufficient for the puncture needle to pass through. Recently, Moran et al. [43] proposed a method involving the direct puncture of the skull and dura mater, as in stereotactic electrode surgery. This method may reduce the loss of cerebrospinal fluid, but the angle of approach may affect the precision of the electrodes. Second, fibrin glue or gelfoam is usually sprayed around the burr holes to minimize CSF loss and air inflow [18, 44, 45]. In our study, we used flowing physiological saline to seal the burr holes, and the mean pneumocephalus volume was 2 cm^3. This result is smaller than that reported in other studies (4–14 cm^3) [31, 44]. A possible reason for this is that the fibrin glue cannot completely seal the burr hole. Due to the effects of intracranial pressure and brain pulsation, CSF will be lost and air will flow in. Although water irrigation cannot completely prevent CSF loss, it can isolate the inside of the cranium from the air. So, flowing physiological saline may be a good way to reduce air inflow. In our study, no correlation between pneumocephalus and accuracy of the electrodes was found, which may be related to the small sample size. Third, intraoperative verification was performed in all patients before electrode implantation, and intraoperative registration was performed before electrode implantation in one patient because the intraoperative verification error had increased. Finally, the implantation time was shortened

because MER was not performed, which is also an important reason.

Seizure Reduction

In our study, the average decrease in seizures was 61% after an average 12-month follow-up. This result was similar to that reported in the literature [7, 10, 11, 13, 14, 46, 47]. Interestingly, two patients with focal clonic seizures (lesion located in the precentral gyrus) in our group achieved a satisfactory seizure reduction (79% and 83%, respectively), but patients with FBTC did not show a significant reduction. Two other patients with focal impaired awareness seizures and FBTC (limbic epilepsy) also demonstrated poor improvements in seizure reduction. This indicated that CMT-DBS may not be effective for FBTC.

Limitations

Given the relatively small sample size of this study, a larger sample size is necessary to confirm the reliability of this method. Another potential limitation of this study is that electrode localization was not confirmed by MER during targeting, and the neurophysiological signature of CMT has shown mixed results in previous studies [12]. Due to the lack of a control group, there may have been a placebo effect or regression to the mean that interfered with the research results. More research is needed to improve identification techniques for thalamic sub-nuclei [10]. Low-frequency stimulation has been reported to improve clinical efficiency [48], and similar research will be done in follow-up work.

CONCLUSION

In this study, frameless robot-assisted asleep surgery was shown to be a precise and safe approach for the placement of CMT electrodes in patients with DRE, shortening surgical times. Segmentation of thalamic nuclei is an efficient method of locating the CMT. Using flowing physiological saline to seal the burr holes is an

excellent way to reduce air inflow. CMT-DBS is an effective method to reduce seizures.

ACKNOWLEDGEMENTS

We thank the participants of the study.

REFERENCES

1. Devinsky O, Vezzani A, O'Brien TJ, Jette N, Scheffer IE, de Curtis M, Perucca P. Epilepsy. Nat Rev Dis Primers. 2018;4:18024. https://doi.org/10.1038/nrdp.2018.24.

2. Beghi E. The epidemiology of epilepsy. Neuroepidemiology. 2020;54:185–91. https://doi.org/10.1159/000503831.

3. Kwan P, Brodie MJ. Early identification of refractory epilepsy. N Engl J Med. 2000;342:314–9. https://doi.org/10.1056/NEJM200002033420503.

4. Slegers RJ, Blumcke I. Low-grade developmental and epilepsy associated brain tumors: a critical update 2020. Acta Neuropathol Commun. 2020;8:27. https://doi.org/10.1186/s40478-020-00904-x.

5. Zheng Z, Jiang H, Wu H, Ding Y, Wang S, Ming W, Zhu J. Epilepsy surgery for low-grade epilepsy-associated neuroepithelial tumor of temporal lobe: a single-institution experience of 61 patients. Neurol Sci. 2021. https://doi.org/10.1007/s10072-021-05703-3.

6. Lamberink HJ, Otte WM, Blümcke I, Braun KPJ. Seizure outcome and use of antiepileptic drugs after epilepsy surgery according to histopathological diagnosis: a retrospective multicentre cohort study. Lancet Neurol. 2020;19:748–57. https://doi.org/10.1016/S1474-4422(20)30220-9.

7. Dalic LJ, Warren AEL, Bulluss KJ, Thevathasan W, Roten A, Churilov L, Archer JS. DBS of thalamic centromedian nucleus for Lennox-Gastaut syndrome (ESTEL Trial). Ann Neurol. 2022;91:253–67. https://doi.org/10.1002/ana.26280.

8. Salanova V, Sperling MR, Gross RE, Irwin CP, Vollhaber JA, Giftakis JE, Fisher RS. The SANTÉ study at 10 years of follow-up: effectiveness, safety, and sudden unexpected death in epilepsy. Epilepsia. 2021;62:1306–17. https://doi.org/10.1111/epi.16895.

9. Vetkas A, Fomenko A, Germann J, Sarica C, Iorio-Morin C, Samuel N, et al. Deep brain stimulation targets in epilepsy: systematic review and meta-analysis of anterior and centromedian thalamic nuclei and hippocampus. Epilepsia. 2022;63:513–24. https://doi.org/10.1111/epi.17157.

10. Cukiert A, Cukiert CM, Burattini JA, Mariani PP. Seizure outcome during bilateral, continuous, thalamic centromedian nuclei deep brain stimulation in patients with generalized epilepsy: a prospective, open-label study. Seizure. 2020;81:304–9. https://doi.org/10.1016/j.seizure.2020.08.028.

11. Son B-C, Shon YM, Choi J-G, Kim J, Ha S-W, Kim S-H, Lee S-H. Clinical outcome of patients with deep brain stimulation of the centromedian thalamic nucleus for refractory epilepsy and location of the active contacts. Stereotact Funct Neurosurg. 2016;94:187–97. https://doi.org/10.1159/000446611.

12. Warren AEL, Dalic LJ, Thevathasan W, Roten A, Bulluss KJ, Archer J. Targeting the centromedian thalamic nucleus for deep brain stimulation. J Neurol Neurosurg Psychiatry. 2020;91:339–49. https://doi.org/10.1136/jnnp-2019-322030.

13. Kim SH, Lim SC, Yang DW, Cho JH, Son B-C, Kim J, et al. Thalamo-cortical network underlying deep brain stimulation of centromedian thalamic nuclei in intractable epilepsy: a multimodal imaging analysis. Neuropsychiatr Dis Treat. 2017;13:2607–19. https://doi.org/10.2147/NDT.S148617.

14. Valentín A, García Navarrete E, Chelvarajah R, Torres C, Navas M, Vico L, et al. Deep brain stimulation of the centromedian thalamic nucleus for the treatment of generalized and frontal epilepsies. Epilepsia. 2013;54:1823–33. https://doi.org/10.1111/epi.12352.

15. Cukiert A, Lehtimäki K. Deep brain stimulation targeting in refractory epilepsy. Epilepsia. 2017;58(Suppl 1):80–4. https://doi.org/10.1111/epi.13686.

16. Velasco AL, Velasco F, Jiménez F, Velasco M, Castro G, Carrillo-Ruiz JD, et al. Neuromodulation of the centromedian thalamic nuclei in the treatment of generalized seizures and the improvement of the quality of life in patients with Lennox–Gastaut syndrome. Epilepsia. 2006;47:1203–12. https://doi.org/10.1111/j.1528-1167.2006.00593.x.

17. Hect JL, Fernandez LD, Welch WP, Abel TJ. Deep brain stimulation of the centromedian thalamic nucleus for the treatment of FIRES. Epilepsia Open. 2022;7:187–93. https://doi.org/10.1002/epi4.12568.

18. Li Z, Zhang J-G, Ye Y, Li X. Review on factors affecting targeting accuracy of deep brain stimulation electrode implantation between 2001 and 2015. Stereotact Funct Neurosurg. 2016;94:351–62. https://doi.org/10.1159/000449206.

19. Neudorfer C, Hunsche S, Hellmich M, El Majdoub F, Maarouf M. Comparative study of robot-assisted versus conventional frame-based deep brain stimulation stereotactic neurosurgery. Stereotact Funct Neurosurg. 2018;96:327–34. https://doi.org/10.1159/000494736.

20. Ribault S, Simon E, Berthiller J, Polo G, Nunes A, Brinzeu A, et al. Comparison of clinical outcomes

and accuracy of electrode placement between robot-assisted and conventional deep brain stimulation of the subthalamic nucleus: a single-center study. Acta Neurochir (Wien). 2021;163:1327–33. https://doi.org/10.1007/s00701-021-04790-7.

21. Yang JC, Bullinger KL, Isbaine F, Alwaki A, Opri E, Willie JT, Gross RE. Centromedian thalamic deep brain stimulation for drug-resistant epilepsy: single-center experience. J Neurosurg. 2022;137: 1591–600. https://doi.org/10.3171/2022.2. JNS212237.

22. Iglesias JE, Insausti R, Lerma-Usabiaga G, Bocchetta M, van Leemput K, Greve DN, et al. A probabilistic atlas of the human thalamic nuclei combining ex vivo MRI and histology. Neuroimage. 2018;183: 314–26. https://doi.org/10.1016/j.neuroimage. 2018.08.012.

23. Fischl B. FreeSurfer. Neuroimage. 2012;62:774–81. https://doi.org/10.1016/j.neuroimage.2012.01.021.

24. Li Y, Wang J, Yang T, Zhang P, Ai K, Li M, et al. Alterations of thalamic nuclei volumes and the intrinsic thalamic structural network in patients with multiple sclerosis-related fatigue. Brain Sci. 2022. https://doi.org/10.3390/brainsci12111538.

25. Liu Q, Wang J, Wang C, Wei F, Zhang C, Wei H, et al. FreeSurfer and 3D slicer-assisted SEEG implantation for drug-resistant epilepsy. Front Neurorobot. 2022;16:848746. https://doi.org/10. 3389/fnbot.2022.848746.

26. Aguado-Carrillo G, Velasco AL, Saucedo-Alvarado PE, Cuellar-Herrera M, Trejo-Martínez D, Navarro-Olvera JL, et al. Radiofrequency ablation of the centromedian thalamic nucleus in the treatment of drug-resistant epilepsy. Epilepsy Behav. 2021;114: 107560. https://doi.org/10.1016/j.yebeh.2020. 107560.

27. Velasco F, Velasco M, Ogarrio C, Fanghanel G. Electrical stimulation of the centromedian thalamic nucleus in the treatment of convulsive seizures: a preliminary report. Epilepsia. 1987;28:421–30. https://doi.org/10.1111/j.1528-1157.1987.tb03668. x.

28. Velasco F, Velasco M, Velasco AL, Jimenez F, Marquez I, Rise M. Electrical stimulation of the centromedian thalamic nucleus in control of seizures: long-term studies. Epilepsia. 1995;36:63–71. https://doi.org/10.1111/j.1528-1157.1995.tb01667. x.

29. Burchiel KJ, McCartney S, Lee A, Raslan AM. Accuracy of deep brain stimulation electrode placement using intraoperative computed tomography without microelectrode recording. J Neurosurg.

2013;119:301–6. https://doi.org/10.3171/2013.4. JNS122324.

30. Goia A, Gilard V, Lefaucheur R, Welter M-L, Maltête D, Derrey S. Accuracy of the robot-assisted procedure in deep brain stimulation. Int J Med Robot. 2019;15:e2032. https://doi.org/10.1002/rcs.2032.

31. Jin H, Gong S, Tao Y, Huo H, Sun X, Song D, et al. A comparative study of asleep and awake deep brain stimulation robot-assisted surgery for Parkinson's disease. NPJ Parkinsons Dis. 2020;6:27. https://doi. org/10.1038/s41531-020-00130-1.

32. Ho AL, Ali R, Connolly ID, Henderson JM, Dhall R, Stein SC, Halpern CH. Awake versus asleep deep brain stimulation for Parkinson's disease: a critical comparison and meta-analysis. J Neurol Neurosurg Psychiatry. 2018;89:687–91. https://doi.org/10. 1136/jnnp-2016-314500.

33. VanSickle D, Volk V, Freeman P, Henry J, Baldwin M, Fitzpatrick CK. Electrode placement accuracy in robot-assisted asleep deep brain stimulation. Ann Biomed Eng. 2019;47:1212–22. https://doi.org/10. 1007/s10439-019-02230-3.

34. Paff M, Wang AS, Phielipp N, Vadera S, Morenkova A, Hermanowicz N, Hsu FPK. Two-year clinical outcomes associated with robotic-assisted subthalamic lead implantation in patients with Parkinson's disease. J Robot Surg. 2020;14:559–65. https:// doi.org/10.1007/s11701-019-01025-x.

35. Furlanetti L, Ellenbogen J, Gimeno H, Ainaga L, Narbad V, Hasegawa H, et al. Targeting accuracy of robot-assisted deep brain stimulation surgery in childhood-onset dystonia: a single-center prospective cohort analysis of 45 consecutive cases. J Neurosurg Pediatr. 2021. https://doi.org/10.3171/2020. 10.PEDS20633.

36. Candela S, Vanegas MI, Darling A, Ortigoza-Escobar JD, Alamar M, Muchart J, et al. Frameless robot-assisted pallidal deep brain stimulation surgery in pediatric patients with movement disorders: precision and short-term clinical results. J Neurosurg Pediatr. 2018;22:416–25. https://doi.org/10.3171/ 2018.5.PEDS1814.

37. Son B-C, Shon Y-M, Kim SH, Kim J, Ko H-C, Choi J-G. Technical implications in revision surgery for deep brain stimulation (DBS) of the thalamus for refractory epilepsy. J Epilepsy Res. 2018;8:12–9. https://doi.org/10.14581/jer.18003.

38. Li J, Li Y, Gutierrez L, Xu W, Wu Y, Liu C, et al. Imaging the centromedian thalamic nucleus using quantitative susceptibility mapping. Front Hum Neurosci. 2019;13:447. https://doi.org/10.3389/ fnhum.2019.00447.

39. Heckemann RA, Hajnal JV, Aljabar P, Rueckert D, Hammers A. Automatic anatomical brain MRI segmentation combining label propagation and decision fusion. Neuroimage. 2006;33:115–26. https://doi.org/10.1016/j.neuroimage.2006.05.061.

40. Fischl B, Salat DH, Busa E, Albert M, Dieterich M, Haselgrove C, et al. Whole brain segmentation: automated labeling of neuroanatomical structures in the human brain. Neuron. 2002;33:341–55. https://doi.org/10.1016/s0896-6273(02)00569-x.

41. Horn A, Li N, Dembek TA, Kappel A, Boulay C, Ewert S, et al. Lead-DBS v2: Towards a comprehensive pipeline for deep brain stimulation imaging. Neuroimage. 2019;184:293–316. https://doi.org/10.1016/j.neuroimage.2018.08.068.

42. de Benedictis A, Trezza A, Carai A, Genovese E, Procaccini E, Messina R, et al. Robot-assisted procedures in pediatric neurosurgery. Neurosurg Focus. 2017;42:E7. https://doi.org/10.3171/2017.2.FOCUS16579.

43. Moran C, Sarangmat N, Gerard CS, Barua N, Ashida R, Woolley M, et al. Two hundred twenty-six consecutive deep brain stimulation electrodes placed using an "Asleep" technique and the Neuro|MateTM Robot for the treatment of movement disorders. Oper Neurosurg (Hagerstown). 2020;19:530–8. https://doi.org/10.1093/ons/opaa176.

44. Piacentino M, Beggio G, Rustemi O, Zambon G, Pilleri M, Raneri F. Pneumocephalus in subthalamic deep brain stimulation for Parkinson's disease: a comparison of two different surgical techniques considering factors conditioning brain shift and target precision. Acta Neurochir (Wien). 2021;163:169–75. https://doi.org/10.1007/s00701-020-04635-9.

45. Hiremath GK. Robotic deep brain stimulation (R-DBS)-"Awake" deep brain stimulation using the neuromate robot and O-arm. Neurol India. 2020;68:S328–32. https://doi.org/10.4103/0028-3886.302450.

46. Cukiert A, Burattini JA, Cukiert CM, Argentoni-Baldochi M, Baise-Zung C, Forster CR, Mello VA. Centro-median stimulation yields additional seizure frequency and attention improvement in patients previously submitted to callosotomy. Seizure. 2009;18:588–92. https://doi.org/10.1016/j.seizure.2009.06.002.

47. Alcala-Zermeno JL, Gregg NM, Wirrell EC, Stead M, Worrell GA, van Gompel JJ, Lundstrom BN. Centromedian thalamic nucleus with or without anterior thalamic nucleus deep brain stimulation for epilepsy in children and adults: a retrospective case series. Seizure. 2021;84:101–7. https://doi.org/10.1016/j.seizure.2020.11.012.

48. Stavropoulos I, Selway R, Hasegawa H, Hughes E, Rittey C, Jiménez-Jiménez D, Valentin A. Low frequency centromedian thalamic nuclei deep brain stimulation for the treatment of super refractory status epilepticus: a case report and a review of the literature. Brain Stimul. 2021;14:226–9. https://doi.org/10.1016/j.brs.2020.12.013.